Radiative Effects on the Diffusional Growth of Ice Particles in Cirrus Clouds

TING WU, WILLIAM R. COTTON, AND WILLIAM Y. Y. CHENG

Department of Atmospheric Science, Colorado State University, Fort Collins, Colorado

(Manuscript received 21 May 1999, in final form 27 September 1999)

ABSTRACT

At Colorado State University the Regional Atmospheric Modeling System (RAMS) has been used to study the radiative effect on the diffusional growth of ice particles in cirrus clouds. Using soundings extracted from a mesoscale simulation of the 26 November 1991 cirrus event, the radiative effect was studied using a two-dimensional cloud-resolving model (CRM) version of RAMS, coupled to an explicit bin-resolving microphysics.

The CRM simulations of the 26 November 1991 cirrus event demonstrate that the radiative impact on the diffusional growth (or sublimation) of ice crystals is significant. Even in a radiatively cooled atmospheric environment, ice particles may experience radiative warming because the net radiation received by an ice particle depends upon the emission from the particle, and the local upwelling and downwelling radiative fluxes.

Model results show that radiative feedbacks on the diffusional growth of ice particles can be very complex. Radiative warming of an ice particle will restrict the particle's diffusional growth. In the case of radiative warming, ice particles larger than a certain size will experience so much radiative warming that surface ice saturation vapor pressures become large enough to cause sublimation of the larger crystals, while smaller crystals are growing by vapor deposition. However, ice mass production can be enhanced in the case of radiative cooling of an ice particle. For the 26 November 1991 cirrus event, radiative feedback results in significant reduction in the total ice mass, especially in the production of large ice crystals, and consequently, both radiative and dynamic properties of the cirrus cloud are significantly affected.

1. Introduction

The climatic importance of cirrus clouds has been recognized for a long time. Cirrus clouds, which cover about 20% of the globe on average, are believed to have profound impacts upon the planetary energy budget due to their radiative effects. Even though during the past decades, the effect of ice clouds on the radiative budget of the earth–atmosphere system has gained considerable impetus in terms of its importance to the World Climate Research Programme, studies of cloud evolution, which ultimately involve the physics of the growth of cloud particles and should hold a special place in cloud–climate research, have not made significant progress because of the complexity of cirrus clouds.

The growth of ice crystals in cirrus clouds has significant consequence because of its contribution to the total diabatic heating or cooling of the atmospheric environment. The microphysical representation of an ice particle's depositional–sublimational growth is usually based on solutions to a set of coupled differential equations that describe a balance between latent heat release associated with deposition of water vapor and heat diffusion, the radiative influence on the particle being ignored. However, the effects of radiation on the growth of ice particles has been postulated to be potentially important.

In the past 20 years, there have been modeling studies on cirrus clouds that have contributed to our understanding of cirrus clouds. Models of various complexity have been used, some with radiative, microphysical, thermodynamical, and dynamical effects, while others may include just the radiative and microphysical effects. Barkstrom (1978) included the effect of radiative transfer in the cloud droplet growth equation. For a cloud base of 2500 m and a cloud top of 3000 m, Barkstrom's results indicated that a droplet can grow from 9.5 to 10.5 μm, 20 times faster when radiative effects are included. Stephens (1983) investigated the effects of radiative heating and cooling on the mass and heat budgets of an ice crystal. Stephens found that radiative cooling enhances ice particle growth, as well as enhances particle fall distances in regions of radiatively cooled upper levels of the cloud. Starr and Cox (1985a,b) used a numerical cloud model to investigate the dynamical, thermodynamical, microphysical, and radiative effects on a thin cirriform cloud formation. Ramaswamy and Detwiler (1986) investigated the interaction of radiation

Corresponding author address: Dr. William Cotton, Department of Atmospheric Science, Colorado State University, Fort Collins, CO 80523-1371.
E-mail: cotton@atmos.colostate.edu

and microphysics in cirrus clouds. They found that for optically thin cirrus, heat diffusion balances latent heating (latent heating and radiative warming) at cloud top (base). For optically thick cirrus, Ramaswamy and Detwiler found that heat diffusion is negligible at cirrus cloud top, but heat diffusion balances latent and radiative heating at cloud base. Zhang et al. (1994) studied the microphysical and radiative properties of cirrus clouds, taking into account the large-scale lifting as well. Zhang et al. (1994) found that small ice crystals can significantly increase the albedo of cirrus clouds, and large-scale lifting can also increase the longevity of cirrus clouds by contributing to an additional cooling.

Using two modeling frameworks, a cloud-resolving model (CRM) and a trajectory parcel model (TPM), Harrington et al. (1999) studied the effects of radiative heating (cooling) on the heat budget, and therefore on the condensational growth, of a population of cloud droplets within an Arctic stratus cloud. His TPM model analysis showed that the radiative effect reduced the time required for the onset of drizzle by up to 30 min in some cases, depending on the cloud-top residence time of the parcels, cloud-top cooling, and the size of the activated drops.

In the aforementioned studies, radiative, microphysical, thermodynamical, and dynamical effects can all play a role in the development of a cirrus cloud. Thus we use a two-dimensional CRM to examine the influence of the radiative heating on the vapor-depositional growth (sublimation) of a population of ice crystals simulated in a CRM of cirrus clouds.

2. Background

Once ice crystals are nucleated by some of the primary or secondary nucleation mechanisms, they then grow by vapor deposition if the environment is supersaturated with respect to ice. The vapor-depositional (or diffusional) growth of ice particles is closely related to the saturation ratio relative to ice, which can be written as

$$S_i = \frac{e}{e_i} = \frac{e}{e_s}\frac{e_s}{e_i} = S\left(\frac{e_s}{e_i}\right), \tag{1}$$

where S denotes the saturation ratio with respect to water; S_i is the saturation ratio with respect to ice; and e, e_i, and e_s denote the environmental vapor pressure, saturation vapor pressure with respect to ice, and saturation vapor pressure with respect to water, respectively.

Since the saturation vapor pressure with respect to water is always greater than that with respect to ice at the same temperature as long as the temperature is below 0°C, a water-saturated ($S = 1$) cloud is always supersaturated with respect to ice ($S_i > 1$) and is a favorable environment for rapid growth of ice crystals by vapor deposition or diffusion. The environment will remain favorable for ice crystal growth as long as liquid drops are available to evaporate and maintain the saturation vapor pressure relative to water. This is commonly known as the Bergeron–Findeisen mechanism.

Traditionally, the diffusional growth of ice crystals follows the Fickian diffusion theory (Rogers and Yau 1989). If the radiative effects are not considered, the diffusional growth equation can be written as (symbols are defined in appendix)

$$\frac{dm_i}{dt} = \frac{4\pi C f_1 f_2 (S_i - 1)}{\dfrac{R_v T}{D e_{si}(T)} + \dfrac{L_s}{KT}\left(\dfrac{L_s}{R_v T} - 1\right)}. \tag{2}$$

However, it has been shown that radiative transfer can have a significant effect on the mass and heat budgets of both ice crystals and cloud droplets (Stephens 1983). In deriving (2), the diffusional growth rate of an ice particle is determined by a steady-state balance between heat released due to deposition and the conduction of heat away from the particle's surface. If it is assumed that the heat release due to sublimation and the energy transferred to the particle by radiation are balanced by the conduction of heat away from the particle, then the diffusional growth equation can be written as (Stephens 1983)

$$L_s \frac{dm_i}{dt} - R = 4\pi C K f_1^* f_2^* (T_r - T_\infty). \tag{3}$$

The total radiative energy absorbed by an ice particle of some characteristic dimension l_R for radiation received over all solid angles ω can be determined by (Stephens 1983)

$$R = \int_0^\infty \int_0^{4\pi} G(l_R, \omega) Q_{\text{abs}}(\lambda, l_R, \omega)(J(T_\Sigma, \lambda, \omega) - B(T_s, \lambda, \omega))\, d\omega\, d\lambda. \tag{4}$$

In (4), Q_{abs} is the particle absorption efficiency, which is a function of the wavelength (λ), the refractive index of ice at that wavelength, and the particle orientation with respect to the incident radiation; $G(l_R, \omega)$ is the geometric cross section of the particle normal to the flow of radiation; and $J(T_\Sigma, \lambda, \omega)$ is the incoming radiation incident on the particle from the surrounding environment at some source temperature T_Σ. This temperature is the same as the environmental temperature T_∞ only for a particle immersed within a blackbody.

$B(T_s, \lambda, \omega)$ is the Planck blackbody function and represents the emission by the particle of temperature T_s at the wavelength λ. The definition of radiative power absorbed by an ice particle as given in (4) involves the integral over all possible directions of incidence (ω) and over all wavelengths (λ).

Utilizing the two-stream approximation in the above integral one gets R for a spherical particle of radius r as (Harrington 1997)

$$R = \int_0^\infty 4\pi r^2 Q_{\text{abs}}(r, \lambda)\left[\pi B(T_s, \lambda) - \frac{1}{2}(F^+ + F^-)\right] d\lambda, \tag{5}$$

where F^+ and F^- are the values of upwelling and downwelling fluxes at wavelength λ. For consistency with the two-stream model, an average value of Q_{abs} for a given spectral band, i, is used and the above equation becomes

$$R_i = 4\pi r^2 \overline{Q}_{\text{abs},i}(\overline{r}_k) E_{d,i}$$

$$E_{d,i} = \left[\pi B_i(T_s) - \frac{1}{2}(F_i^+ + F_i^-)\right], \tag{6}$$

where $\overline{Q}_{\text{abs},i}(\overline{r}_k)$ is the absorption coefficient averaged over spectral band i and computed at the mean size of microphysical bin number k as to be discussed; F_i^+ and F_i^- are the values of fluxes for band i; and $B_i(T_s)$ is the band-integrated Planck function evaluated at the particle's surface temperature. The total radiative effect R can be obtained by summing up R_i over the total number of microphysical bins.

Now, it is straightforward to get the total radiative energy absorbed by a particle of size $\overline{r}_k$ as

$$R = 4\pi \overline{r}_k^2 \sum_{i=1}^{N_{\text{bands}}} \overline{Q}_{\text{abs},i}(\overline{r}_k) E_{d,i}, \tag{7}$$

where N_{bands} is the total number of radiation bands used in the radiation model. In order to evaluate the radiative effects on particle's diffusional growth in the explicit microphysical model, the radiative term shown above is included in the model equations for supersaturation and for the growth of particle. These equations are solved together in a manner that ensures self-consistency.

3. Model description

The model used to examine the radiative effects on ice particle's diffusional growth is a coupling of the Regional Atmospheric Modeling System CRM with the bin-resolving microphysics model developed at the University of Tel Aviv (Tzivion et al. 1987, 1989; Reisin 1995; Reisin et al. 1996; Feingold et al. 1996). It is a two-dimensional version of the large eddy simulation model described in detail in Stevens et al. (1996a) and Feingold et al. (1996). The strength of this model lies in its emphasis on both dynamics and microphysics through the coupling of the bin-resolving microphysical model with a dynamical model that resolves the large eddies. A detailed description of the coupled code for the liquid phase microphysics can be seen in Stevens et al. (1996a,b). Reisin (1995) and Reisin et al. (1996) provide a detailed description of the mixed-phase microphysics model. To accommodate the inclusion of radiative effects, the current version of the model couples the optical properties of the droplets and ice particles to an eight-band radiative transfer model developed by Harrington (1997; see also Harrington et al. 1999; Olsson et al. 1998).

Although the two-dimensional model does not represent the eddy structure as well as its three-dimensional large eddy simulation counterpart, it does include the essential interactions between large eddies and cloud microphysical processes as well as the radiative feedback and provides a valuable framework for testing hypotheses without enormous computational expense (Stevens et al. 1998).

The level-5 mixed-phase bin-microphysical representation of this model requires that equations for droplet activation, condensational/evaporational growth, collision–coalescence of drops, ice nucleation, deposition and sublimation of ice crystals, collision–coalescence of ice particles, and sedimentation all be explicitly modeled. The decision on which processes are to be included in the model is based upon a number of factors (Reisin 1995):

- the importance of the process to the relevant problem studied;
- the availability of relevant data such as collision efficiencies, terminal velocities, shape factors, etc.; and
- limitations on computational resources.

The ice-phase microphysics is based on the work of Reisin (1995) and Reisin et al. (1996). Currently, three ice species named pristine ice (PI), snow (aggregates), and graupel are included in the bin-microphysics representation of the model. Ice crystals in the model are created by nucleation of ice nuclei or by freezing of drops smaller that 100 μm in radius. The specific shape of the ice particles is assumed to be plates (approximated by oblate spheroids) for PI and spheres for snow and graupel. Snow particles are formed by aggregation of ice crystals and are considered to have the minimum density (0.2 g cm^{-3}) compared with pristine ice crystals (0.7 g cm^{-3}) and graupel (0.5 g cm^{-3}). Graupel particles are formed by freezing of drops with radii larger than 100 μm and/or by different processes of particle coagulation. Ice crystals of different sizes are categorized into different bins (to be described below).

The liquid-phase microphysics is based on Feingold et al. (1994) and Stevens et al. (1996a,b), allowing growth by condensation, evaporation, and collision–coalescence (through the use of stochastic collection equation). This scheme explicitly resolves the size spectrum

TABLE 1. Bin number and particle size relation for the first 25 bins. The particle sizes are in cm.

Bin	Rain	Pristine ice	Graupel	Aggregate
1	0.31250E−03	0.35195E−03	0.39373E−03	0.53437E−03
2	0.39373E−03	0.44343E−03	0.49606E−03	0.67326E−03
3	0.49606E−03	0.55869E−03	0.62500E−03	0.84826E−03
4	0.62500E−03	0.70390E−03	0.78745E−03	0.10687E−02
5	0.78745E−03	0.88686E−03	0.99213E−03	0.13465E−02
6	0.99213E−03	0.11174E−02	0.12500E−02	0.16965E−02
7	0.12500E−02	0.14078E−02	0.15749E−02	0.21375E−02
8	0.15749E−02	0.17737E−02	0.19843E−02	0.26930E−02
9	0.19843E−02	0.22348E−02	0.25000E−02	0.33930E−02
10	0.25000E−02	0.28156E−02	0.31498E−02	0.42749E−02
11	0.31498E−02	0.35475E−02	0.39685E−02	0.53861E−02
12	0.39685E−02	0.44695E−02	0.50000E−02	0.67860E−02
13	0.50000E−02	0.56312E−02	0.62996E−02	0.85499E−02
14	0.62996E−02	0.70949E−02	0.79370E−02	0.10772E−01
15	0.79370E−02	0.89390E−02	0.10000E−01	0.13572E−01
16	0.10000E−01	0.11262E−01	0.12599E−01	0.17100E−01
17	0.12599E−01	0.14190E−01	0.15874E−01	0.21544E−01
18	0.15874E−01	0.17878E−01	0.20000E−01	0.27144E−01
19	0.20000E−01	0.22525E−01	0.25198E−01	0.34200E−01
20	0.25198E−01	0.28380E−01	0.31748E−01	0.43089E−01
21	0.31748E−01	0.35756E−01	0.40000E−01	0.54288E−01
22	0.40000E−01	0.45050E−01	0.50397E−01	0.68399E−01
23	0.50397E−01	0.56759E−01	0.63496E−01	0.86177E−01
24	0.63496E−01	0.71512E−01	0.80000E−01	0.10858E+00
25	0.80000E−01	0.90100E−01	0.10079E+00	0.13680E+00

of cloud condensation nuclei. The number of newly activated droplets is determined from the supersaturation (from Kohler theory). Like the ice crystals, droplets of different sizes are categorized into different bins (see below).

The particle spectra for any category are divided into 25 bins (x_k, $k = 1, \ldots, 25$) with mass doubled in the next larger bin:

$$x_{k+1} = 2x_k. \tag{8}$$

The initial mass is $x_1 = 1.598 \times 10^{-11}$ g for any category, which corresponds to a diameter of 3.125 μm for drops, 3.520 μm for pristine ice crystals, 3.937 μm for graupel particles, and 5.344 μm for aggregates. The size of each category at bin 25 is 800 μm for drops, 901 μm for pristine ice crystals, 1008 μm for graupel, and 1368 μm for aggregates. Table 1 shows the size–bin information for bins from 1 to 25. The number of total bins can be larger or smaller than 25, depending upon the specific cases. These spectra shown in the table are adequate for simulating midlatitude cirrus clouds.

The evolution of the supersaturation with respect to both water and ice is prognosticated, and the radiative effect on the diffusional growth (or evaporation) of drops and ice particles can be turned on and/or off in order to test its importance.

The two-stream radiation model (Harrington 1997; Harrington et al. 1999; Olsson et al. 1998) is coupled to the bin-microphysics model, solving for radiative transfer of H_2O, O_3, and CO_2 and the optical effects of the hydrometeor size spectra. An advantage of this model is that it considers three different classes of ice crystals: hexagonal plates, hexagonal columns, and bullet rosettes (five branches). The geometry (via the ratio of volume to projected area) of the ice crystals is computed using the algorithm in Mitchell and Arnott (1994). This radiation scheme has been tested against gamma distribution for which analytical solutions are known, and the error never exceeds 2%.

4. CRM simulation results

The sounding used to drive the CRM simulations was extracted from a mesoscale simulation of the 26 November 1991 First International Satellite Cloud Climatology Project (ISCCP) Regional Experiment (FIRE) II cirrus event (Wu 1999) and is shown in Fig. 1. Since the bin microphysics has the advantage of predicting particle size–dependent supersaturation with respect to water as well as ice, it is quite suitable for the study of the radiative effects on ice crystal vapor-depositional growth in cirrus clouds.

In order to examine radiative effects on ice particle diffusional growth, two simulations were performed. In one of the simulations, the radiative effect was added to the particle's diffusional growth equation as well as the supersaturation equation, while in the other simulation, radiative feedback was turned off.

Figures 2–5 compare the CRM simulated supersaturation with respect to ice (SSI), water vapor mixing ratio, PI number concentration, snow (aggregate) number concentration, and total ice mass. It is seen in Fig. 2 that a maximum SSI of more than 23% is produced in the simulation with radiative feedback, while in the simulation without radiative feedback the maximum SSI predicted is generally less than 3%. Also, it is apparent

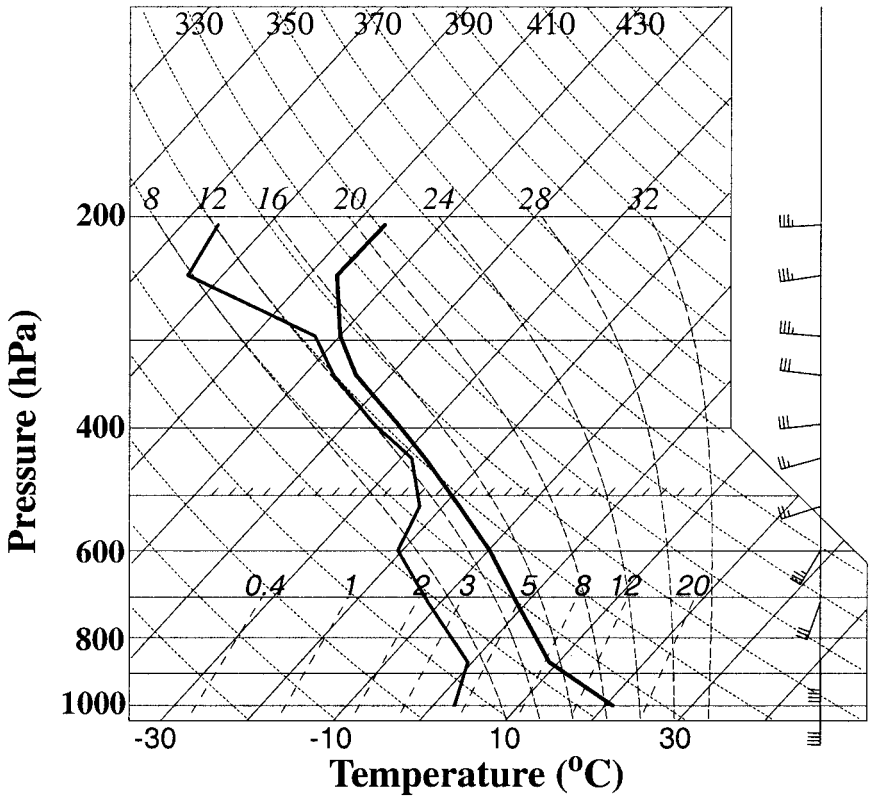

FIG. 1. Skew *T*-log*P* diagram for temperature (°C), and wind (m s^{-1}) at intial time of the CRM simulation.

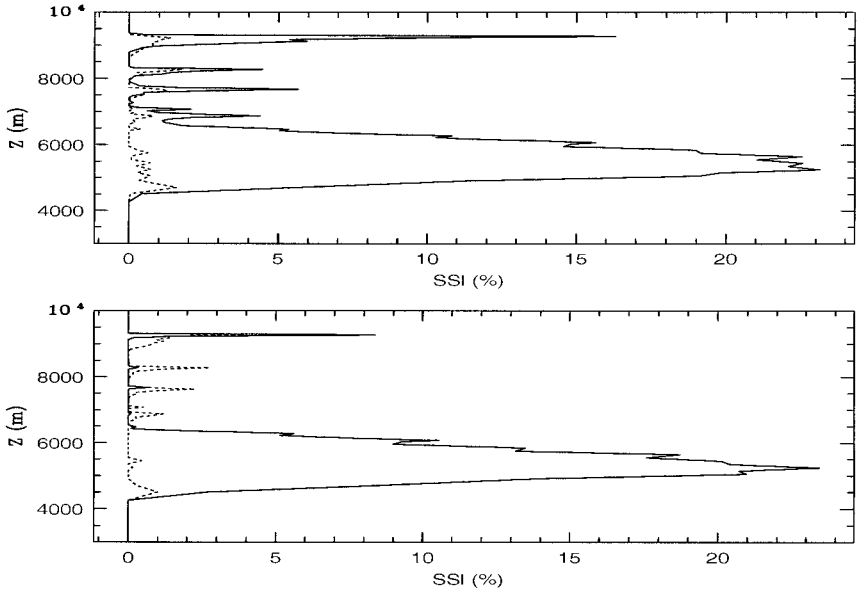

FIG. 2. Profiles of domain-averaged supersaturation with respect to ice at 30 (top) and 60 min (bottom) into the simulations (solid line, with radiative feedback; dotted line, without radiative feedback).

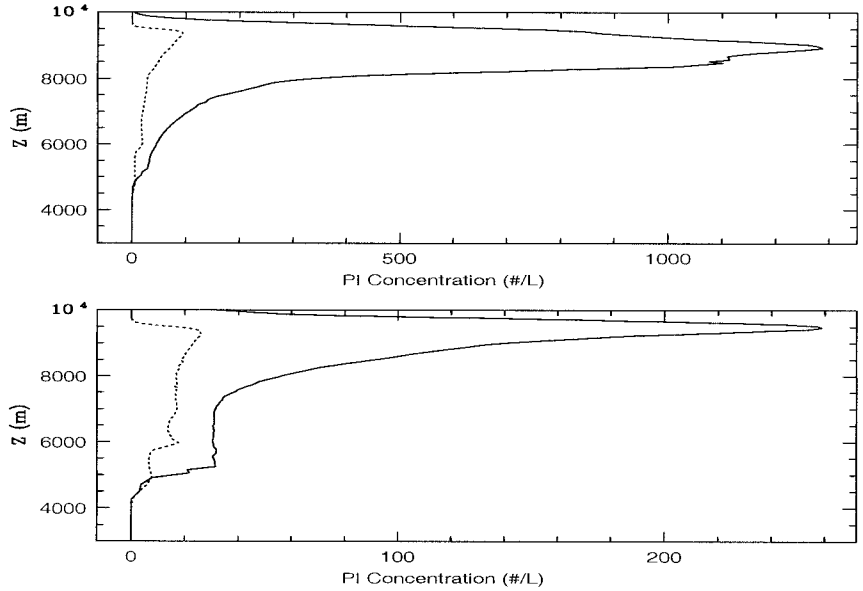

FIG. 3. Profiles of domain-averaged PI number concentration at 30 (top) and 60 min (bottom) into the simulations (solid line, with radiative feedback; dotted line, without radiative feedback).

that the largest jump in SSI production occurs in the lower levels of the cloud. In response to greater SSI production, a maximum PI concentration of nearly 1300 L^{-1} is predicted near the cloud top at 30 min into the simulation with radiative feedback. This compares to the maximum PI concentration of less than 100 L^{-1} in the simulation without radiative feedback (Fig. 3) at the same time. In contrast to the massive production of PI in the simulation with radiative feedback, Fig. 4 shows that maximum aggregate number concentration produced in this simulation has dropped significantly from about 8.0×10^{-5} L^{-1} (in the simulation without radiative feedback) to slightly more than 2.0×10^{-5} L^{-1}. As the simulation proceeds from 30 to 60 min, the number concentration of PI has reduced dramatically, while the maximum snow particle number concentration has increased by a factor of about 6. This is because aggregation of PI particles results in production of snow.

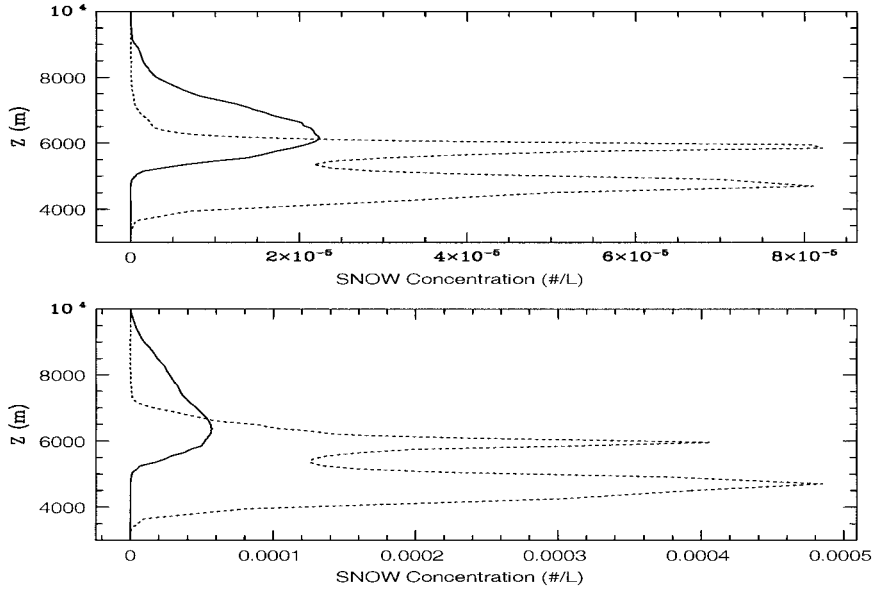

FIG. 4. Profiles of domain-averaged snow particle number (SNOW) concentration at 30 (top) and 60 min (bottom) into the simulations (solid line, with radiative feedback; dotted line, without radiative feedback).

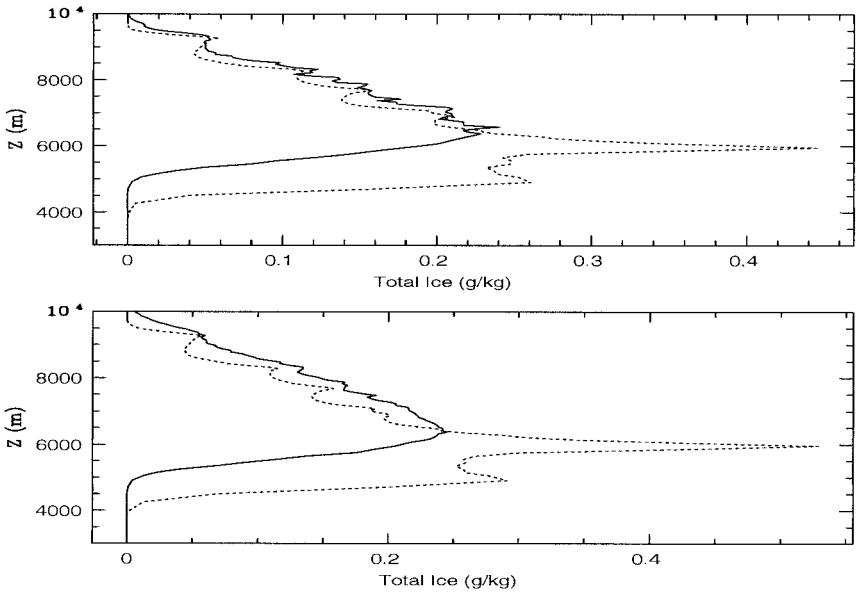

FIG. 5. Profiles of domain-averaged total ice at 30 (top) and 60 min (bottom) into the simulations (solid line, with radiative feedback; dotted line, without radiative feedback).

Also evident is that most aggregate particles in the simulation without radiative feedback reside near the cloud base (below 6-km level), while in the simulation with radiative feedback, most of the aggregate particles are deep in the cloud layer between 5.2- and 8-km levels.

Even though much more PI crystals are produced in the simulation with radiative feedback than in the simulation without radiative feedback, the maximum PI mixing ratio (0.24 g kg^{-1}) predicted in the simulation with radiative feedback is only about half of the value (0.42 g kg^{-1}) produced in the other simulation. Following a similar trend as in the PI mixing ratio prediction, maximum aggregate mixing ratio predicted in the simulation with radiative feedback (3×10^{-7} g kg^{-1}) is more than one order less than predicted in simulation without radiative feedback (1.5×10^{-5} g kg^{-1}) at 30 min of simulation time. Figure 5 compares the total ice predicted for the two simulations at 30 and 60 min of simulation time. It is evident that much less ice mass is produced in the simulation with radiative feedback compared to the prediction without radiative feedback, in terms of peak values as well as in the average values. At 30 min into the simulation, the average total ice mixing ratio between 4 and 10 km is 0.09 g kg^{-1} (0.13 g kg^{-1}) with (without) radiative feedback. At 60 min into the simulation, the average total ice mixing ratio between 4 and 10 km is 0.1 g kg^{-1} (0.15 g kg^{-1}) with (without) radiative feedback.

Figure 6 shows the particle size–dependent radiative flux toward a particle at 100 time steps for a parcel that has its origin at 4038.0 m, while Fig. 7 displays the radiative flux for another parcel whose origin is deep in the cloud layer at 7013.47 m above the ground. The results show that radiative warming (mainly from shortwave) of ice particles (see bottom panels of Figs. 6 and 7) is dominant in the cloud layer. Also smaller ice particles tend to experience less shortwave radiative warming than larger particles in the simulation with radiative feedback. It should be noted that radiative warming or cooling for an ice particle is different from the warming or cooling of the atmospheric environment because one depends on the balance described by Eq. (4) (for a particle) while the other depends on the divergence of the net radiative fluxes (upwelling plus downwelling). So, when the model predicts that the atmosphere experiences radiative cooling, it does not necessarily imply that each particle sees the same effect because as these two figures display, radiative warming or cooling for a particle is size dependent.

Based upon Figs. 6 and 7, one can explain the lack of ice production in the simulation with radiative feedback easily. High SSI activates the ice nucleation processes in the bin-microphysics model. The ice particles produced through nucleation processes are added to the relevant bins (always very small bins) of the PI category. After the formation of these ice particles, they experience diffusional growth in an environment of positive SSI. The newly nucleated ice crystals are so small that the radiative effect is not a significant factor in the early stage of an ice particle's diffusional growth.

As more and more PI crystals are produced, collision and coalescence among the ice particles result in the formation of aggregates. Both aggregates and PI crystals can experience significant growth through diffusion of water vapor as long as $-R$ in Eq. (3) is not enough to balance the right-hand side (note that R is negative for radiative warming). On attaining a certain size (e.g., r_{limit}), an ice particle finds itself in a situation in which

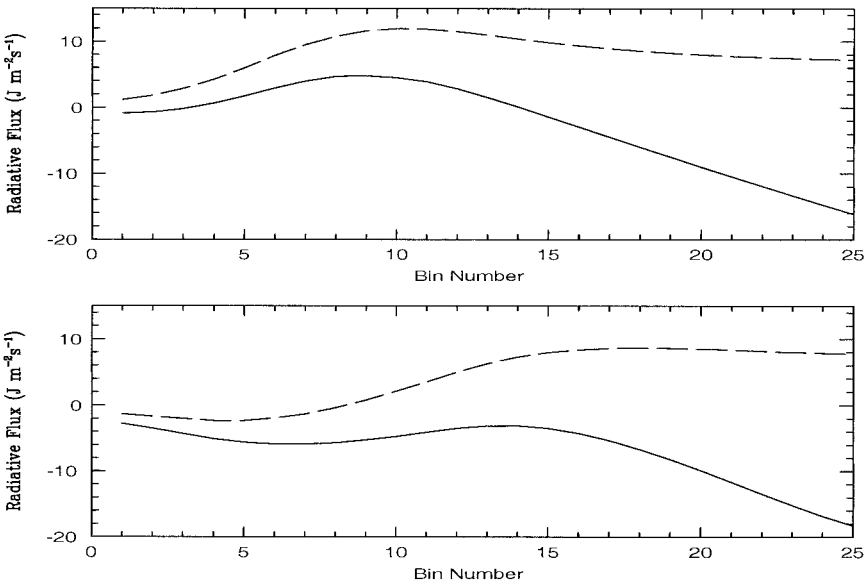

FIG. 6. Examples of bin-dependent radiative flux toward water (top) and ice (bottom) particles at 100 timesteps (δt = 2 s) for a parcel originated near the cloud base. Positive flux denotes radiative cooling, while negative denotes radiative warming (solid lines, longwave plus shortwave; dashed lines, longwave only).

the radiation it absorbs is balanced by the diffusion of heat away from the particle's surface and diffusional growth is substantially retarded because the saturation vapor pressure at the particle's surface is enhanced. However, particles larger than r_{limit} can be produced through aggregation, but these larger particles cannot survive for very long because the radiation they absorb maintains high values of surface ice saturation vapor pressures. Eventually, particles larger than r_{limit} will warm sufficiently to experience evaporation, which adds water vapor to the free air, resulting in higher water mixing ratio (or supersaturation with respect to ice), especially in the region between 4- and 6-km levels. Large ice particles in the simulation without radiative

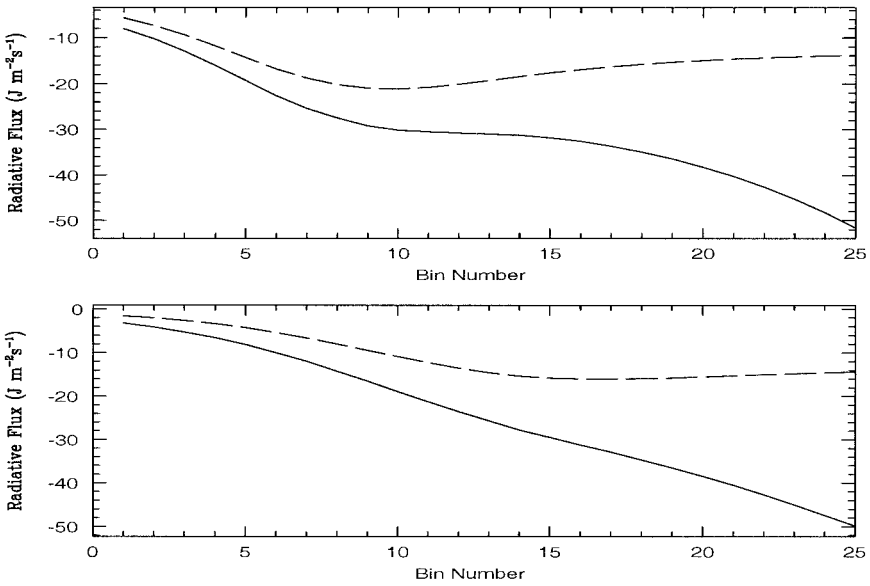

FIG. 7. Examples of bin-dependent radiative flux toward water (top) and ice (bottom) particles at 100 time steps (δt = 2 s) for a parcel originated deep in the cloud layer. Positive flux denotes radiative cooling, while negative denotes radiative warming (solid lines, longwave plus shortwave; dashed lines, longwave only).

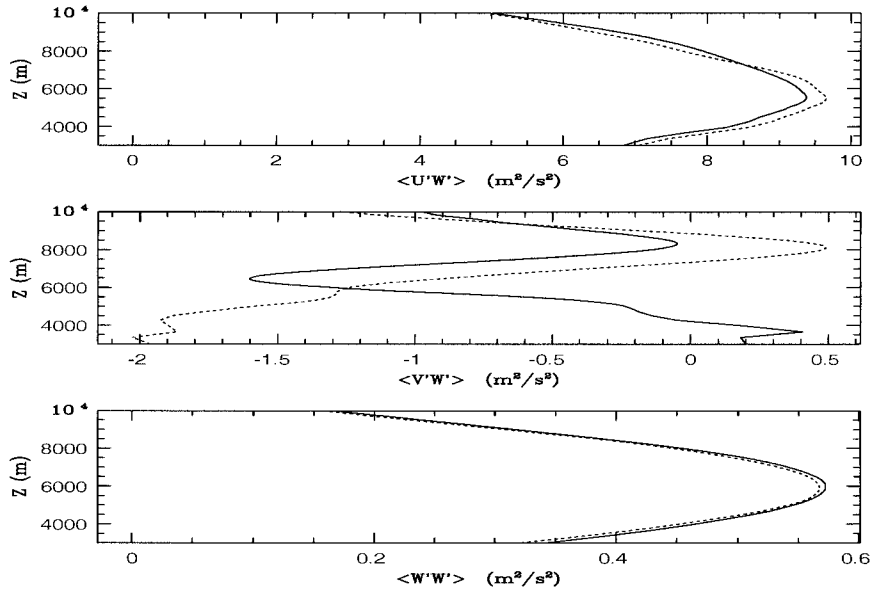

FIG. 8. Momentum flux profiles at 60 min of simulation time. The solid line and dotted line are for runs with and without radiative feedback, respectively.

feedback, however, are not restricted in their vapor depositional growth by the processes stated above. This is the reason why more ice mass production is predicted in the simulation without radiative feedback than in the simulation with radiative feedback.

Fluxes of momentum, θ_{il}, and r_t are also compared between the simulation with radiative feedback and that without radiative feedback (see Figs. 8 and 9). The two simulations have generally similar vertical profiles for these fluxes, except that $\langle V'W' \rangle$ displays significant difference below 6-km level. The larger absolute magnitude in $\langle V'W' \rangle$ associated with the simulation without radiative feedback may indicate that more active entrainment and detrainment processes are involved. This conclusion is supported by the larger $\langle r_t'W' \rangle$ near the cloud base for the simulation without radiative feedback.

Figure 10 compares the total turbulent kinetic energy (TKE) and TKE production between the two simulations. The total TKE profile indicates that the simulation without radiative feedback tends to be more turbulent than the simulation with radiative feedback, especially

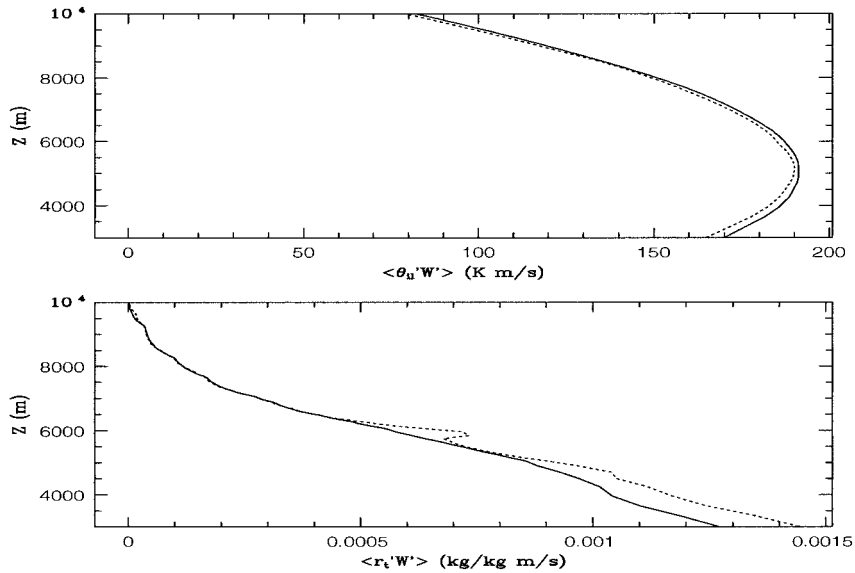

FIG. 9. Profiles of $\langle \theta_{il}'W' \rangle$ and $\langle r_t'W' \rangle$ at 60 min of simulation time. The solid line and dotted line are for runs with and without radiative feedback, respectively.

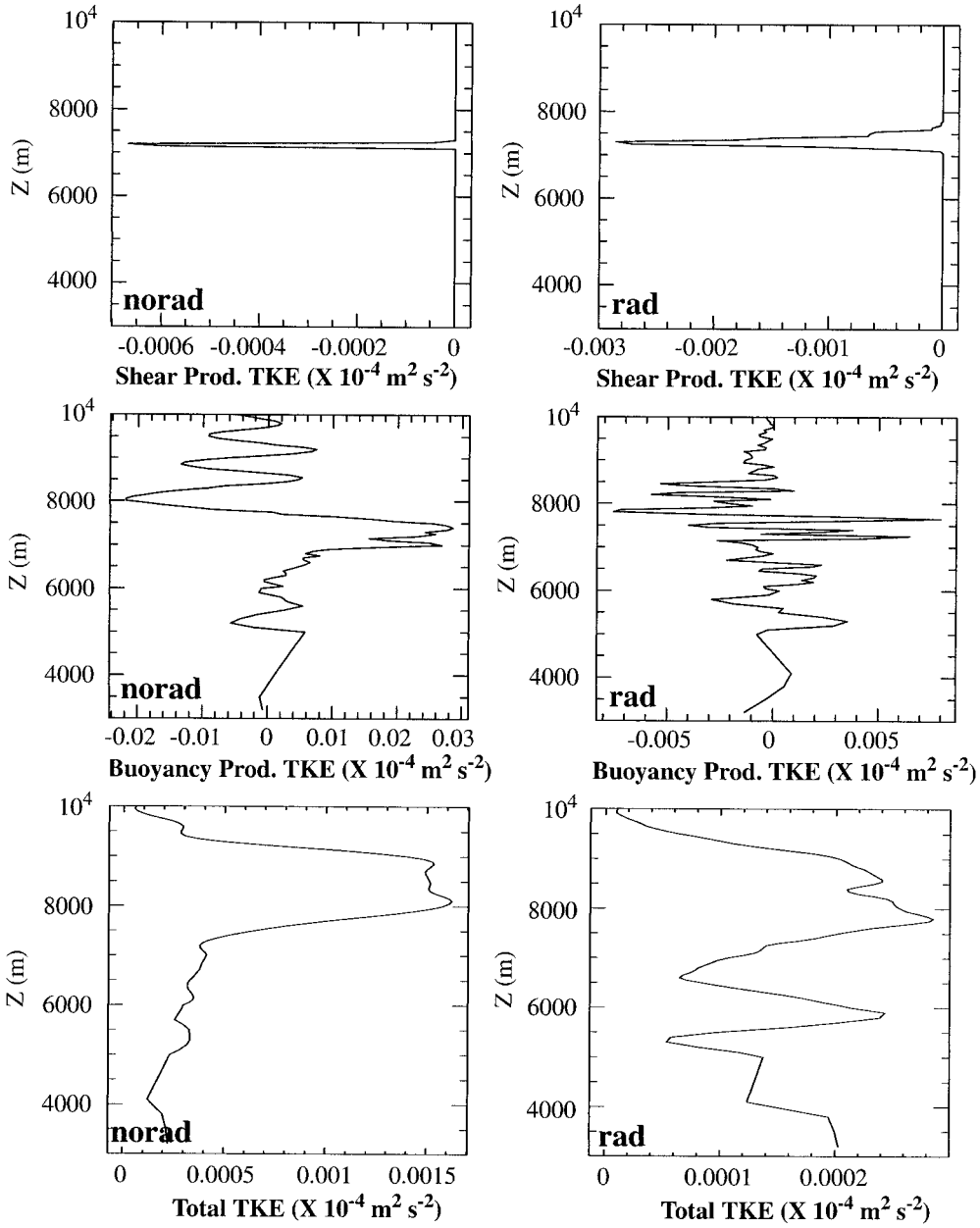

FIG. 10. Profiles of total TKE and TKE production terms for the simulations without (left panel) and with (right panel) radiative feedback on particle's diffusional growth at 60 min of the simulation time.

in the upper levels of the cloud system. Generally, the upper levels of the cloud system tend to be negatively buoyant, while below 7700 m, positive buoyancy dominates for the simulation without radiative feedback. Also, shear production, which is not a significant factor compared with buoyancy production, is confined to a very shallow region between 7500 and 7700 m for this simulation. However, for the simulation with radiative feedback, shear production is comparable to buoyancy in the very shallow region similar to that in the other simulation. The appearance of layered structures in the total TKE profiles for the case with radiative feedback suggests that the cloud system is more decoupled in the vertical for the simulation with radiative feedback than for the simulation without radiative feedback.

Consistent with the difference in ice mass production, the optical depths (both solar as well as infrared) predicted in the simulation without radiative feedback are larger than that predicted in the simulation with radiative feedback (Fig. 11). The two peaks near 5 and 6 km in the optical-depth profiles correspond very well to the peaks in aggregate and PI production, respectively.

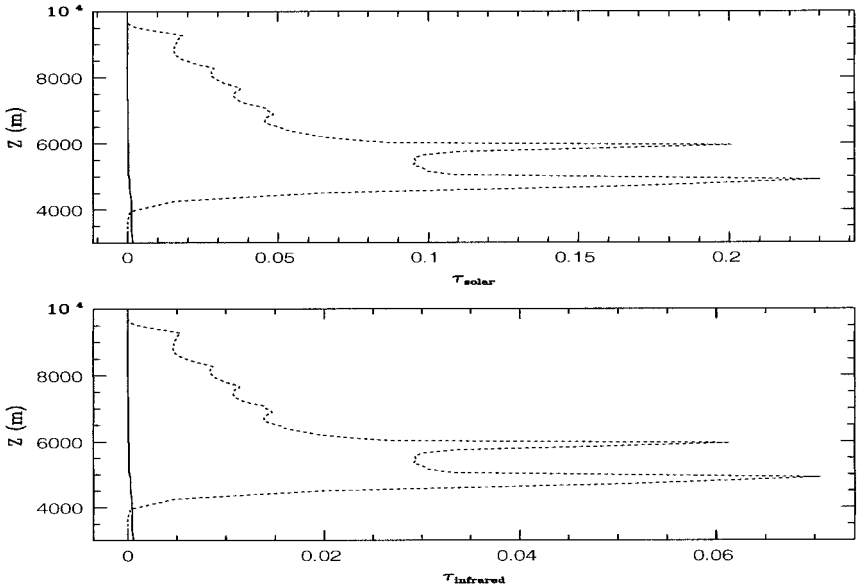

FIG. 11. Profiles of solar (τ_{solar}) and infrared (τ_{infrared}) optical depths at 60 min of simulation time. The solid line and dotted line are for runs with and without radiative feedback, respectively.

Since the model-predicted cloud system without radiative feedback is optically thick and consists of larger ice particles than the cloud predicted in the simulation with radiative feedback, Fig. 12 shows that a well-defined pattern of upper-level cooling and lower-level warming dominates the simulation without radiative feedback because the cloud system is able to absorb more longwave radiation from below (resulting in warming near cloud base) and emits more longwave radiation near cloud top, which results in more radiative cooling above than in the simulation with radiative feedback. In the simulation with radiative feedback, since the model-predicted cloud system is optically thinner, solar radiation can penetrate deeper into the cloud layer than in the simulation without radiative feedback, resulting in a peak of solar warming just below the 6000-m level. Both cooling and warming in the simulation without radiative feedback are more significant than in the

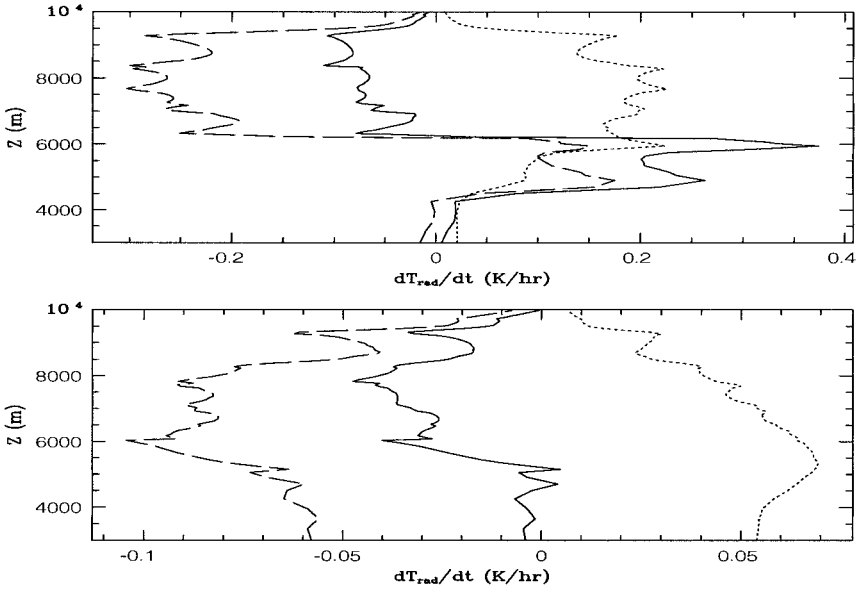

FIG. 12. Profiles of total (solid), infrared (dashed), and solar (dotted) radiative heating rates at 60 min of simulation time. (top) Without radiative feedback on particles' diffusional growth; (bottom) with radiative feedback.

other simulation just because of the significant difference in the optical depth of the model-predicted clouds.

5. Summary

CRM simulations of the 26 November 1991 FIRE II cirrus event demonstrate that the radiative effects on an ice particle's diffusional growth (or evaporation) can significantly affect the macrostructure and microstructure of cirrus clouds. However, the radiative impact on the evolution and properties of cirrus clouds can be very complex. Radiative warming for an ice particle will restrict the particle's diffusional growth. In the case of radiative warming, saturation vapor pressure on the surface of ice crystals can increase to the point that vapor deposition growth is retarded or changed to sublimation. However, ice mass production can be enhanced in the case of net radiative cooling of an ice particle.

Further sensitivity tests of the radiative effects on ice particle's diffusional growth should be done for different cirrus cloud regimes using the CRM and large eddy simulation frameworks. Even though the CRM simulations of this study have shown significant difference between the simulations with radiative feedback and that without radiative feedback, it should be remembered that the simulation results apply only to this specific case.

Acknowledgments. This work was supported by the National Aeronautics and Space Administration under Contracts NAG-1-1703 and NAG-1-2045. Jerry Harrington and Tamir Reisin are acknowledged for their critique of the derivations in the text. The help of Brenda Thompson in preparing this manuscript is greatly appreciated.

APPENDIX

Definition of Symbols

C	Capacity
c_p	Specific heat at constant pressure
D	Molecular diffusion coefficient
e_{si}	Saturation vapor pressure with respect to ice
e_{sw}	Saturation vapor pressure with respect to water
f_1	Ventilation factor
f_2	Gas kinetic factor
K	Thermal conductivity of air
L_c	Latent heat of condensation
L_s	Latent heat of sublimation
M_i	Total ice mass due to depositional growth
M_w	Total liquid mass due to condensational growth
m_i	Mass of a single ice particle
m_w	Mass of a single water droplet
q_v	Specific humidity (water vapor mixing ratio)
q_{si}	Saturation water vapor mixing ratio with respect to ice
q_{sw}	Saturation water vapor mixing ratio with respect to water
R	Longwave radiative energy
R_v	Gas constant for water vapor
r	Radius of a particle
S_i	Saturation ratio with respect to ice
ΔS_i	Specific humidity surplus with respect to ice
S_w	Saturation ratio with respect to water
ΔS_w	Specific humidity surplus with respect to water
T	Air temperature
T_r	Temperature at the surface of a particle
T_∞	Environmental temperature (is equal to T)
$\rho_{s,r}$	Saturation (to water) vapor density at the surface of a particle
$\rho_{si,r}$	Saturation (to ice) vapor density at the surface of a particle
ρ_∞	Environmental vapor density

REFERENCES

Barkstrom, B., 1978: Some effects of 8–12 μm radiant energy transfer on the mass and heat budgets of cloud droplets. *J. Atmos. Sci.,* **35,** 665–673.

Feingold, G., B. Stevens, W. R. Cotton, and A. S. Frisch, 1996: The relationship between drop in-cloud residence time and drizzle production in numerically simulated stratocumulus clouds. *J. Atmos. Sci.*, **53,** 1108–1122.

Harrington, J. Y., 1997: The effects of radiative and microphysical processes on simulated warm and transition-season Arctic stratus. Ph.D. dissertation, Colorado State University, 270 pp. [Available from Dept. of Atmospheric Science, Colorado State University, Fort Collins, CO 80523.]

——, T. Reisin, W. R. Cotton, and S. M. Kreidenweis, 1999: Cloud resolving simulations of Arctic stratus. Part II: Transition-season clouds. *Atmos. Res.,* **51,** 45–75.

Mitchell, D. L., and W. P. Arnott, 1994: A model predicting the evolution of ice particle size spectra and radiative properties of cirrus clouds. Part II: Dependence of absorption and extinction on ice crystal morphology. *J. Atmos. Sci.,* **51,** 817–832.

Olsson, P. Q., J. Y. Harrington, G. Feingold, W. R. Cotton, and S. Kreidenweis, 1998: Exploratory cloud-resolving simulations of boundary layer Arctic stratus clouds. Part I: Warm season clouds. *Atmos. Res.,* **47–48,** 573–597.

Ramaswamy, V., and A. Detwiler, 1986: Interdependence of microphysics and radiation in cirrus clouds. *Atmos. Res.,* **43,** 2289–2301.

Reisin, T., 1995: A numerical study of cloud seeding in Israel using as axisymmetrical cloud model with detailed microphysics. Ph.D. dissertation, Department of Geophysics and Planetary Sciences, Tel Aviv University, 238 pp. [Available from Dept. of Geophysics and Planetary Science, Tel Aviv University, Ramat Aviv 69978, Israel.]

——, Z. Levin, and S. Tzivion, 1996: Rain production in convective clouds as simulated in an axisymmetric model with detailed microphysics. Part I: Description of the model. *J. Atmos. Sci.,* **53,** 497–519.

Rogers, R. R., and M. K. Yau, 1989: *A Short Course in Cloud Physics.* 3d ed. Pergamon Press, 293 pp.

Starr, D. O'C., and S. K. Cox, 1985a: Cirrus clouds. Part I: A cirrus cloud model. *J. Atmos. Sci.,* **42,** 2663–2681.

——, and ——, 1985b: Cirrus clouds. Part II: Numerical experiments on the formation and maintenance of cirrus. *J. Atmos. Sci.,* **42,** 2682–2694.

Stephens, G. L., 1983: The influence of radiative transfer on the mass and heat budgets of ice crystals in the atmosphere. *J. Atmos. Sci.,* **40,** 1729–1739.

Stevens, B., G. Feingold, W. R. Cotton, and R. L. Walko, 1996a:

Elements of the microphysical structure of numerically simulated nonprecipitating stratocumulus. *J. Atmos. Sci.,* **53,** 980–1007.

——, R. L. Walko, W. R. Cotton, and G. Feingold, 1996b: The spurious production of cloud-edge supersaturations by Eulerian models. *Mon. Wea. Rev.,* **124,** 1034–1041.

——, W. R. Cotton, and G. Feingold, 1998: A critique of one- and two-dimensional models of boundary layer clouds with a binned representation of drop microphysics. *Atmos. Res.,* **47–48,** 529–553.

Tzivion, S., G. Feingold, and Z. Levin, 1987: An efficient numerical solution to the stochastic collection equation. *J. Atmos. Sci.,* **44,** 3139–3149.

——, ——, and ——, 1989: The evolution of raindrop spectra. Part II: Collisional collection/breakup and evaporation in a rainshaft. *J. Atmos. Sci.,* **46,** 3312–3327.

Wu, T., 1999: Numerical modeling study of the November 26, 1991 cirrus event. Ph.D. dissertation, Colorado State University, 186 pp. [Available from Dept. of Atmospheric Science, Colorado State University, Fort Collins, CO 80523.]

Zhang, Y., M. Laube, and E. Raschke, 1994: Numerical simulation of cirrus properties. *Beitr. Phys. Atmos.,* **67,** 109–120.